© 2014. Published by The Company of Biologists Ltd | Development (2014) 141, 2895-2900 doi:10.1242/dev.107730

RESEARCH REPORT

TECHNIQUES AND RESOURCES

Quantitative 4D analyses of epithelial folding during *Drosophila* gastrulation

Zia Khan[1,*], Yu-Chiun Wang[2,3,4], Eric F. Wieschaus[3,4] and Matthias Kaschube[5,*]

ABSTRACT

Understanding the cellular and mechanical processes that underlie the shape changes of individual cells and their collective behaviors in a tissue during dynamic and complex morphogenetic events is currently one of the major frontiers in developmental biology. The advent of high-speed time-lapse microscopy and its use in monitoring the cellular events in fluorescently labeled developing organisms demonstrate tremendous promise in establishing detailed descriptions of these events and could potentially provide a foundation for subsequent hypothesis-driven research strategies. However, obtaining quantitative measurements of dynamic shapes and behaviors of cells and tissues in a rapidly developing metazoan embryo using time-lapse 3D microscopy remains technically challenging, with the main hurdle being the shortage of robust imaging processing and analysis tools. We have developed EDGE4D, a software tool for segmenting and tracking membrane-labeled cells using multi-photon microscopy data. Our results demonstrate that EDGE4D enables quantification of the dynamics of cell shape changes, cell interfaces and neighbor relations at single-cell resolution during a complex epithelial folding event in the early *Drosophila* embryo. We expect this tool to be broadly useful for the analysis of epithelial cell geometries and movements in a wide variety of developmental contexts.

KEY WORDS: *Drosophila melanogaster*, Epithelial folding, Cell shape reconstruction, Live imaging, Cell tracking, Cell shape analysis

INTRODUCTION

Complex and dynamic cell shape changes and movements occur during morphogenetic events. These events are crucial for tissue construction during embryonic development and for organ formation during post-embryonic stages (Lecuit and Lenne, 2007; Paluch and Heisenberg, 2009). Whereas a fair amount is known about the underlying patterning mechanism in several model systems, much less is understood about the molecular, cellular and mechanical factors that control cell and tissue shapes. Quantitative analyses of cell shapes and subcellular events using 4D (x, y, z and time) imaging approaches promise to hold the key to an improved understanding of tissue morphogenesis (Oates et al., 2009; Keller, 2013).

Fluorescent membrane markers are widely used for imaging the shape dynamics of densely arranged cells in developing tissues. Despite the ease with which these markers can be imaged, no generally applicable computational tool is available for the accurate reconstruction, tracking and analysis of these cells. This is in part because general-purpose, automated cell reconstruction and tracking remains an ill-posed computational problem. Thus, achieving the accuracy of the human visual system remains challenging (Khairy and Keller, 2011).

Yet, progress can be made using computational methods tailored to subclasses of membrane-label data. Using this approach, quantitative measurements of 3D cell shape have been demonstrated in the plant meristem (Fernandez et al., 2010; Federici et al., 2012). In metazoans, tools have focused on early developmental stages of zebrafish and ascidians, the morphologies of which are relatively simple and in which cell movement is limited (Olivier et al., 2010; Sherrard et al., 2010). For processes that display greater morphological changes, cell shape is often ignored and nuclei are used as a proxy for cell position (McMahon et al., 2008; Giurumescu et al., 2012). In cases in which the cell shape is computationally analyzed, 2D measurements from planar optical slices of a tissue have been used to approximate 3D measurements of cell shapes (Blanchard et al., 2009; Gelbart et al., 2012). Recently, true 3D computational methods have been successfully applied to somite formation in zebrafish to reconstruct cells that exhibit complex shapes. These cells, however, undergo only limited displacements (Mosaliganti et al., 2012). Here, we demonstrate computational methods that enable 3D quantitative analyses of cell shape change during an epithelial folding event in which cells undergo dramatic morphological changes and display large and rapid displacement.

RESULTS AND DISCUSSION

We have made our methods and data available as an open-source software tool called EDGE4D (https://sites.google.com/site/edge4dsupplement). EDGE4D incorporates all stages of processing including image filtering, segmentation, cell tracking and quantitative analyses. We used dorsal fold formation, an epithelial folding event that occurs during *Drosophila* gastrulation, to develop EDGE4D. Dorsal fold formation takes place within a time frame of 30 min. Cells undergo multiple types of shape change and extensive movements, ultimately producing two epithelial folds: the anterior and the posterior fold (Wang et al., 2012, 2013). Because of the rapid pace of cell shape change and the depth of the final tissue structure, time-lapse 3D microscopy data of dorsal fold formation are challenging to analyze due to low signal-to-noise imaging conditions. To address the challenges associated with these data, we developed several novel algorithmic strategies (outlined in detail in the supplementary material methods). Specifically, we contribute: an approach for repairing signal along the outside of the tissue structure; a geometric strategy for cell segmentation that is robust to small breaks in membrane detection; and an approach that allows the identification of cell-cell contact surfaces

[1]Center for Bioinformatics and Computational Biology, University of Maryland, College Park, MD 20742, USA. [2]RIKEN Center for Developmental Biology, 2-2-3 Minatojima-minamimachi, Chuo-ku, Kobe-shi, Hyogo-ken 650-0047, Japan. [3]Department of Molecular Biology, Princeton University, Princeton, NJ 08544, USA. [4]The Howard Hughes Medical Institute, Moffett Laboratory 435, Princeton University, Princeton, NJ 08544, USA. [5]Frankfurt Institute for Advanced Studies, Faculty of Computer Science and Mathematics, Goethe University, Frankfurt am Main D-60438, Germany.

*Authors for correspondence (zia@cs.umd.edu; kaschube@fias.uni-frankfurt.de)

Received 2 January 2014; Accepted 19 May 2014

Development (2014) 141, 2895-2900 doi:10.1242/dev.107730

that uses the duality between surface meshes and binary image volumes.

We began developing EDGE4D using single-photon confocal laser scanning microscopy on fixed embryos labeled for cell membrane and nuclei at high spatial resolution across three developmental stages of fold formation (Fig. 1A). Since the segmentation of nuclei was unambiguous (Fig. 1B; supplementary material Movie 1), providing a ground truth for cell identification, we matched nuclei with segmented cell shapes to assess segmentation errors. Among several hundred cells that we analyzed, we found that the segmentation error rate based on membrane label alone was less than 4% (Fig. 1C). By contrast, segmentation of cell membrane using the core segmentation algorithm of a previous approach developed for reconstructing cells from plant meristems (Fernandez et al., 2010) resulted in a high rate of missed cells (MARS-ALT in Fig. 1C), as the approach could not accurately detect cells that have incomplete membrane label signal (red arrows, Fig. 1A). Another approach developed for studying zebrafish somite formation missed many cells and generated a higher rate of broken cells (ACME in Fig. 1C). Our results indicate that these approaches, which are tailored to different developmental systems, could not be directly applied to data collected from the *Drosophila* dorsal folds.

Next, we evaluated the quality of segmentations that EDGE4D produced by computing the root mean squared (RMS) error between hand-drawn segmentations of cells in orthogonal slices through the data versus the corresponding slices through EDGE4D-generated segmentations (supplementary material Fig. S1). Errors in both our manual segmentations and in our EDGE4D segmentations contribute to the RMS error. Therefore, to provide a baseline, we also computed the RMS error between unambiguously segmented nuclei and hand-drawn segmentations. We found that the RMS error in the shapes of the cells is no worse than that in the shapes of nuclei despite the close contact and more complex shapes of the cells ($P>0.05$, one-sided Wilcoxon rank-sum; supplementary material Fig. S2). Our results illustrate that EDGE4D can accurately detect and reconstruct cell shapes from membrane labels.

We next extended EDGE4D to process time-lapse 3D data collected using two-photon laser scanning microscopy on living embryos, in which membrane and nuclei were labeled separately with distinct fluorescent protein fusion constructs (Fig. 1D; supplementary material Movie 2). Similar to the analysis performed on the fixed embryos, segmentation using EDGE4D resulted in fewer missed and broken cells than MARS-ALT or ACME, indicating that these previous computational methods could not be directly applied to our time-lapse data (Fig. 1E,F). The low overall error rate of EDGE4D on a second, independently collected data set illustrated that our results were reproducible (supplementary material Fig. S4). Overall, segmentation of cells in the live data was more challenging due to a decrease in the signal-to-noise ratio and lower *z*-resolution (supplementary material Fig. S3). Therefore, we introduced an additional extension in EDGE4D that combines information from the nuclear and membrane channels such that ambiguity in one channel (e.g. membrane) was corrected by information from the other (e.g. nuclei; see supplementary material methods). A simple assay of the number of time points that each cell was tracked suggested that this extension improves the handling of noise in these data (Fig. 1G; $P<10^{-15}$, Wilcoxon rank-sum).

A crucial test for a 4D analysis tool is its ability to reliably track cells. We evaluated this functionality of EDGE4D based on the neighbor relations of cells. Since cells undergo minimal neighbor exchange and do not divide during dorsal fold formation, EDGE4D should report stable cell-cell contacts if the cell tracking is accurate (Fig. 1H). To evaluate neighbor stability, we analyzed 347 tracked cell trajectories that spanned ten or more consecutive time points. For each trajectory, we ranked neighbors of a given cell trajectory based on the duration of contact and computed the percentage of the trajectory within which the contact was stably maintained. We found that the five top-ranked neighbors maintain their association with the focal cell nearly 90% of the time, whereas the duration of contact drops to just below 70% for the sixth-ranked neighbors. Given that these densely packed columnar epithelial cells are predominantly hexagonal and often have six neighboring cells, this analysis suggests that the cell tracking is highly robust (Fig. 1I; supplementary material Figs S5, S6). We also counted events in which more than half the neighbors of a cell changed, which is likely to indicate a tracking error. In this analysis we observed a low rate of errors, and only at later time points (Fig. 1J). Overall, these results indicate that EDGE4D can robustly track cells in noisy live data, allowing us to reliably analyze individual cell behaviors throughout the process of dorsal fold formation. We note that EDGE4D does not explicitly use neighbor stability information during tracking and is not limited to systems with stable cell neighbors. Moreover, the analyses establish a novel, yet potentially generalizable approach of using stable cell-cell contacts to evaluate the accuracy of cell tracking. Other developmental systems that also exhibit minimal degrees of neighbor exchange could be used to establish our evaluation approach as a benchmark standard.

Since EDGE4D identifies and tracks cells reliably, we used it to explore cell geometry during dorsal fold formation. We focused on cells that move to the basalmost part of each dorsal fold, as they undergo the largest vertical displacement (Fig. 2A; supplementary material Movie 3). These basalmost cells belong to a group called initiating cells that display a basal shift of the positioning of adherens junctions and a subsequent apical-basal shortening (Wang et al., 2012). Such localized shape changes in an otherwise uniform sheet of epithelium could in principle provide the necessary forces to induce tissue deformation and subsequent folding. Importantly, however, such cell shape changes would have a stronger effect on the neighboring cells to induce tissue deformation if the volume of individual cells remains constant. We tested this hypothesis and found that, although the basalmost cells undergo significant apical-basal shortening, we could not detect statistically significant changes in volume. These results suggest that the basalmost cells might obey the principle of volume conservation during apical-basal shortening and that this cell shape change might exert forces to induce tissue bending (Gelbart et al., 2012) (Fig. 2B). Our results demonstrate the potential of EDGE4D to uncover important features of tissue morphogenesis at single-cell resolution.

Having established that EDGE4D can be used to analyze cell shape changes, we explored its ability to quantify cell contacts. In addition to apical-basal shortening, the initiating cells and their immediate neighbors appear to undergo anisotropic shape change in the plane of the epithelium: their cross-sectional aspect ratio increased significantly from $t=0$ to $t=800$ s, skewing toward the dorsal-ventral axis (Fig. 2C; $P<10^{-12}$, Wilcoxon rank-sum). These observations suggest that the contact surface areas might also become anisotropic. To test this prediction, we used EDGE4D to first define individual contact surfaces between initiating cells and their neighbors using a novel algorithm that we developed which uses the duality between surface meshes and binary image volumes (see supplementary material methods). We then measured their surface areas directly (Fig. 2D; supplementary material Movie 4). Consistent with our prediction, the areas of the contact surfaces parallel to the dorsal-ventral axis increased, whereas those oriented parallel to the anterior-posterior axis decreased (Fig. 2E,F). Based

Development (2014) 141, 2895-2900 doi:10.1242/dev.107730

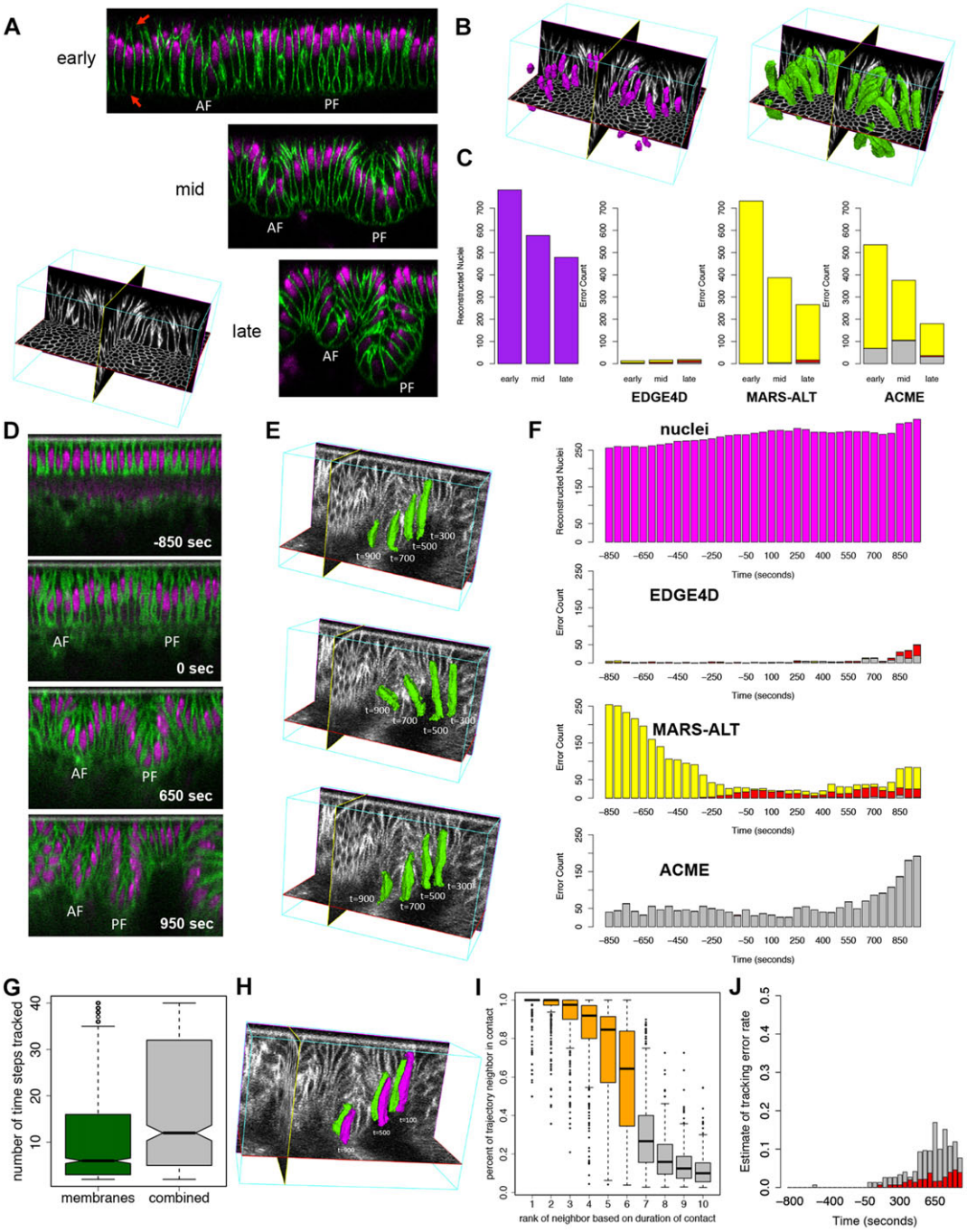

Fig. 1. Assessment of cell shape reconstruction and tracking. (A) Mid-sagittal slices of the dorsal folds from fixed *Drosophila* embryos staged at early, mid and late stages. AF, anterior fold; PF, posterior fold. Membranes were labeled by antibody to Neurotactin and nuclei by OliGreen DNA dye. The red arrows highlight missing membrane signal along the basal and apical ends of the cells. (B) Examples of a subset of nuclei (purple) and cell shapes (green) reconstructed from the mid-stage fixed data set. Based on their nuclei, virtually all cells could be correctly identified, providing a ground truth for testing their identification based on membrane labeling alone. (C) Quantification of the number of nuclei (purple) at each stage. The greater number of nuclei at the early time point is due to the larger field of view. Error counts are shown for EDGE4D, MARS-ALT and ACME applied to only the membrane channel in the data sets. Merged cells (red), broken cells (gray) and missed cells (yellow) were detected using the nuclei. (D) Mid-sagittal slices of the dorsal folds from a live data set collected using two-photon imaging. Time 0 s designates the completion of cellularization. Membranes were labeled with *Resille-GFP* and nuclei were labeled with *H2Av-mRFP*. (E) Examples of three different cells tracked into the posterior fold. Cell shapes are shown for time points 300 s, 500 s, 700 s and 900 s past completion of cellularization in the live two-photon data set. (F) Segmentation error counts across the time points collected. Merged cells (red), broken cells (gray) and missed cells (yellow) were detected using the nuclei reconstructions as ground truth. (G) The number of time points that a cell was tracked using the membrane channel alone (green) or the combined membrane and nuclear signal (gray). (H) Example of two cells that maintain stable contact as they descend into the posterior fold at 100 s, 500 s and 900 s past the completion of cellularization. (I) Analysis of neighbor contact stability for 211 cells tracked for more than ten time points. (G,I) The ends of the boxes are the quartiles; the centerline is the median; notches, where present, provide the 95% confidence interval around the median; and whiskers extend 1.5 times the interquartile range. (J) Assessment of the tracking error rate based on the number of events in which more than half the neighbors of a cell changed for cells tracked ten time points or more using membrane signal only (gray) or membrane and nuclei (red).

Development (2014) 141, 2895-2900 doi:10.1242/dev.107730

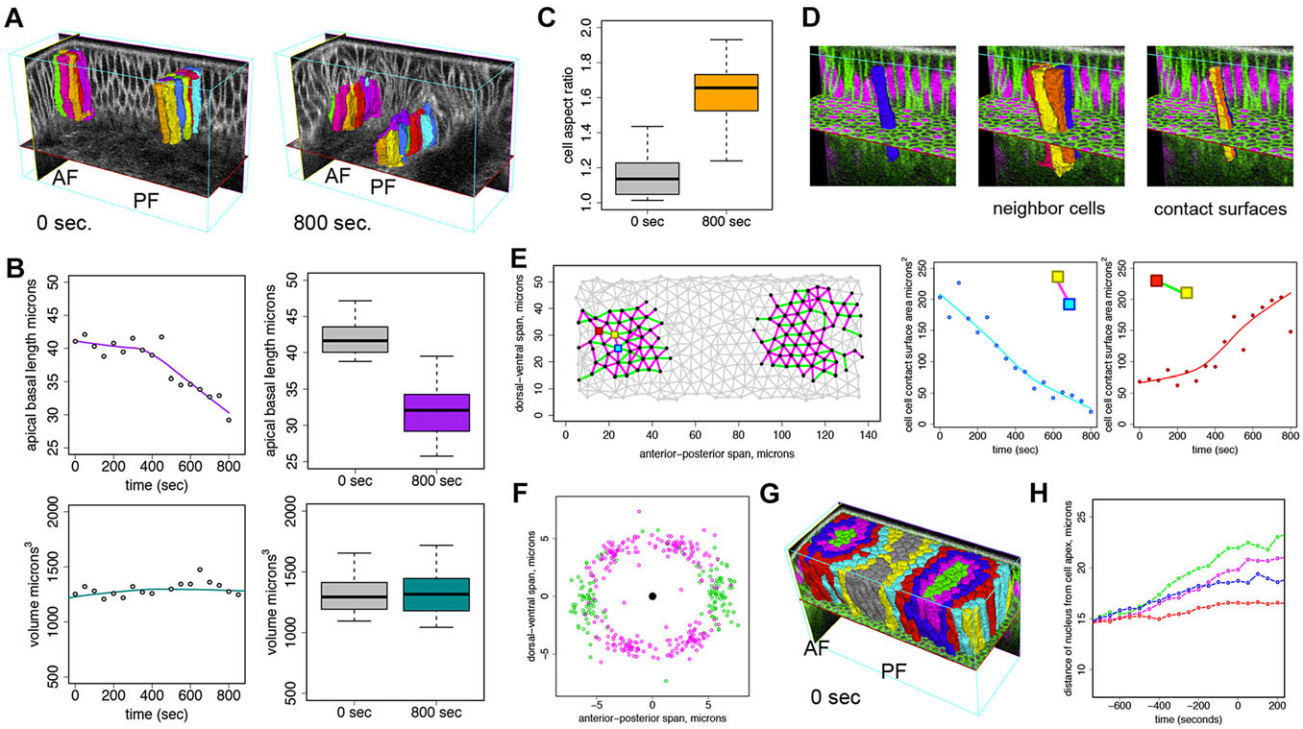

Fig. 2. Quantitative 4D analyses of cells in the dorsal folds. (A) Basalmost initiating cells tracked into the anterior and posterior folds between 0 s and 800 s past the completion of cellularization. Colors designate the same cell between these two time points. (B) (Left) Example of smoothed traces of apical-basal length and volume for an individual cell. Gray points designate actual measurements. (Right) Boxplots of apical-basal cell length at the completion of cellularization (t=0 s) and at t=800 s for N=29 basalmost initiating cells. (C) The aspect ratio of basalmost initiating cells as measured manually using ImageJ from 2D z-stacks through the dorsal folds. (B,C) The ends of the boxes are the quartiles; the centerline is the median; and whiskers extend 1.5 times the interquartile range. (D) An example of a segmented cell (left) and its neighbors (middle). The contact surfaces of the cell (right) have been colored according to the colors of its neighbors. (E) (Left) Cell-cell contacts at the completion of cellularization (t=0 s) are indicated by edges in the graph. Nodes are positioned at projected cell centroids. Only cell-cell contacts between basalmost initiating cells and their first and second degree neighbors that were reliably tracked between t=0 s and t=800 s and that remained in the field of view were analyzed. Purple edges designate cell-cell contacts among these cells that decrease in surface area, and green edges designate cell-cell contacts that increase in surface area at 800 s. (Center and right) Smooth traces of cell contact surface area for the designated cell-cell contacts, as indicated by the colored squares in the left figure. Points correspond to actual surface area measurements. (F) Distribution of cell surface centroids relative to the projected cell centroid (center black point) at the completion of cellularization (t=0 s) for basalmost initiating cells and their first and second degree neighbors. Purple points designate the positions of contact surfaces that decrease in area at t=800 s past cellularization; green points designate the position of surfaces that increase in area at t=800 s relative to the focal cell. (G) Cells are labeled based on their neighbor relationship to the basalmost initiating cells (green). (H) Median distance of nuclei from the cell apices over time for the basalmost cells and their neighbors. Note that neighbors along the edge of the field of view were not analyzed.

on these new measurements, we hypothesize that either adhesive or contractile forces within the cells become increasingly anisotropic or that these cells are under compressing or stretching forces exerted externally along the two major axes. Although further experimental work will be necessary to test these mechanical hypotheses, EDGE4D quantitation represents, to our knowledge, the first dynamic 3D analysis of cell contact surfaces.

Lastly, we assessed the ability of EDGE4D to analyze the dynamics of subcellular events. As a first step, we found that nuclei co-migrate with junctions towards the basal side of the initiating cells, suggesting that nuclear positioning could be used as a proxy for the position of the junctions (supplementary material Fig. S7, Movie 5). To systematically analyze nuclear positioning, we used the neighbor relations functionality in EDGE4D to define distinct cell groups relative to the basalmost cells (green, Fig. 2G). We then used EDGE4D to monitor the distance between nuclei and cell apexes in each group of cells (see supplementary material methods). While the nuclei of the initiating cells, including the basalmost cells (green) and their first (magenta) and second (blue) degree neighbors, move basally prior to the completion of cellularization, the nuclei of the neighboring cells (red) remain apically positioned (Fig. 2H). These analyses confirm our previous observations, obtained from manual measurements of 2D midsagittal optical sections, that a change in the apical-basal polarity occurs specifically in the initiating cells and not in the neighboring cells (Wang et al., 2012).

EDGE4D demonstrates systematic cell reconstruction and quantitative analyses of cell shape during the rapid and dynamic events of dorsal fold formation in *Drosophila* gastrulation. We have made EDGE4D available as an open-source tool in order that others will benefit from, as well as contribute to, its methods and algorithms, as we extend and adapt these computational techniques to a broader range of developmental systems and contexts. At present, EDGE4D does not directly handle actively dividing cells. However, we expect that integration with existing lineage analysis techniques will allow EDGE4D to analyze this class of cells (Bao et al., 2006). Our own efforts using the techniques underlying EDGE4D to analyze *Drosophila* tracheal cells provide evidence that these methods can be generalized to other developmental systems (Nelson et al., 2012). However, our experience suggests that adapting these methods to other systems requires some expert knowledge of the underlying image processing steps. Semi-supervised machine learning techniques might improve EDGE4D in this regard (Szeliski, 2011).

Development (2014) 141, 2895-2900 doi:10.1242/dev.107730

In conclusion, advances in time-lapse imaging technologies, such as two-photon and planar illumination microscopy (Truong et al., 2011; Gao et al., 2012; Krzic et al., 2012; Tomer et al., 2012), continue to improve our ability to perform 3D imaging of dynamic tissue morphogenesis with greater depth and at higher temporal and spatial resolution. However, the promise of these technologies as powerful tools of discovery can only be fulfilled with the parallel development of image processing and quantitation tools that allow the extraction of quantitative measurements from time-lapse 3D imaging data. EDGE4D represents a major step forward in this direction.

MATERIALS AND METHODS

Fly stocks, sample preparation and microscopy

For fixed embryos, the *Oregon-R* strain was used. The embryos were fixed with the heat-methanol method (Müller and Wieschaus, 1996). The cell membrane was labeled with anti-Neurotactin (BP106, Developmental Studies Hybridoma Bank, 1:20) followed by an Alexa Fluor 633-conjugated goat anti-mouse secondary antibody (Molecular Probes, A-21052, 1:500). The nuclei were labeled with OliGreen DNA dye (Molecular Probes, 1:5000). *z*-stack images of fixed embryos were taken on a Leica SP5 spectral confocal system using a 63× multi-immersion objective with argon 488 and a He-Ne 633 lasers. Voxel size was d_x=0.16023 µm, d_y=0.16023 µm, d_z=0.12588 µm and the (*x*,*y*,*z*) dimensions of the imaging regions were 164×82×52 µm, 103×82×61 µm and 79 µm×82 µm×68 µm for the early, mid and late stage data sets, respectively. For two-color live imaging, flies containing the *Resille-GFP* protein trap (Morin et al., 2001) (also known as *P{PTT-un1}CG8668*$^{117\text{-}2}$) and the *H2Av-mRFP* transgene (Pandey et al., 2005) (also known as *P{His2Av-mRFP1}*) were used to label membrane and nuclei, whereas flies containing the *H2Av-GFP* transgene (Clarkson and Saint, 1999) (also known as *P{His2Av*$^{T:Avic\backslash GFP\text{-}S65T}$*}*) and the *E-Cadherin-GFP* transgene (Oda and Tsukita, 2001) were used to label nuclei and junctions. These embryos were dechorionated in commercial bleach, affixed to a glass slide using home-made embryo glue (a heptane-based adhesive made from Scotch double-sided tape), and immersed in water. Two-photon time-lapse imaging was performed on a custom-made system built on an upright Olympus BX51 microscope equipped with a piezo-driven long-range objective scanner (Physik Instrumente) for fast *z*-stack generation using a 40× water-immersion objective. A Chameleon Ti:sapphire tunable laser (Coherent) was tuned at 960 nm for simultaneous excitation of the green and red fluorescent proteins. Voxel size was d_x=0.559 µm, d_y=0.625 µm, d_z=0.5 µm and the (*x*,*y*,*z*) dimensions of the imaging region were 149×59.6×90 µm. Image stacks were acquired every 50 s. Raw image data are available for download at: https://sites.google.com/site/edge4dsupplement/data.

EDGE4D implementation and availability

Source code for EDGE4D can be downloaded from: https://sites.google.com/site/edge4dsupplement. EDGE4D is implemented in C++ and depends on the open-source Qt (http://qt-project.org), libTIFF (http://www.remotesensing.org/libtiff) and OpenGL (through the Qt library). We have also provided the raw data and R (http://www.r-project.org) scripts used to generate the results in this study. The raw data sets include the parameters used for analysis in XML format. We provide an overview of EDGE4D in the supplementary material methods. The source code provides precise implementation details. We recommend a computer with at least 16 GB of RAM for processing the live data set. Data processing of the live data set takes 16 min on a 1.6 GHz 8-core Intel Xeon E5603 with 72 GB of RAM using 8 CPU threads. We have provided a subset of the live data that can be processed on a computer with 8 GB of RAM. We expect to continue improving the performance of EDGE4D. We hope that by providing the complete source code of EDGE4D we also provide a convenient framework through which new approaches for quantitative 4D analyses could be developed.

Computational methods

A detailed description of the computational methods is provided in the supplementary material methods.

Acknowledgements

We thank Stephan Thiberge for assistance with two-photon microscopy. We also thank Mona Singh for her helpful comments on early versions of EDGE4D.

Competing interests

The authors declare no competing financial interests.

Author contributions

Z.K. and M.K. devised the segmentation and tracking methods. Z.K. implemented the software and designed and conducted the analyses with input from Y.-C.W., E.F.W. and M.K. Y.-C.W. optimized the labeling and imaging conditions and collected the raw imaging data and assisted in designing the analyses. All authors jointly conceived the study in its design and coordination. Z.K., Y.-C.W. and M.K. wrote the paper. All authors read and approved the final manuscript.

Funding

This work was funded by grants from the National Institutes of Health (NIH) [P50 GM071508 (PI: D. Botstein to Z.K. and M.K.) and 5R37HD015587 to E.F.W.]; the Howard Hughes Medical Institute (E.F.W.); and a Helen Hay Whitney Research Fellowship (Y.-C.W.). Deposited in PMC for release after 6 months.

Supplementary material

Supplementary material available online at
http://dev.biologists.org/lookup/suppl/doi:10.1242/dev.107730/-/DC1

References

Bao, Z., Murray, J. I., Boyle, T., Ooi, S. L., Sandel, M. J. and Waterston, R. H. (2006). Automated cell lineage tracing in Caenorhabditis elegans. *Proc. Natl. Acad. Sci. U.S.A.* **103**, 2707-2712.

Blanchard, G. B., Kabla, A. J., Schultz, N. L., Butler, L. C., Sanson, B., Gorfinkiel, N., Mahadevan, L. and Adams, R. J. (2009). Tissue tectonics: morphogenetic strain rates, cell shape change and intercalation. *Nat. Methods* **6**, 458-464.

Clarkson, M. and Saint, R. (1999). A His2AvDGFP fusion gene complements a lethal His2AvD mutant allele and provides an in vivo marker for Drosophila chromosome behavior. *DNA Cell Biol.* **18**, 457-462.

Federici, F., Dupuy, L., Laplaze, L., Heisler, M. and Haseloff, J. (2012). Integrated genetic and computation methods for in planta cytometry. *Nat. Methods* **9**, 483-485.

Fernandez, R., Das, P., Mirabet, V., Moscardi, E., Traas, J., Verdeil, J.-L., Malandain, G. and Godin, C. (2010). Imaging plant growth in 4D: robust tissue reconstruction and lineaging at cell resolution. *Nat. Methods* **7**, 547-553.

Gao, L., Shao, L., Higgins, C. D., Poulton, J. S., Peifer, M., Davidson, M. W., Wu, X., Goldstein, B. and Betzig, E. (2012). Noninvasive imaging beyond the diffraction limit of 3D dynamics in thickly fluorescent specimens. *Cell* **151**, 1370-1385.

Gelbart, M. A., He, B., Martin, A. C., Thiberge, S. Y., Wieschaus, E. F. and Kaschube, M. (2012). Volume conservation principle involved in cell lengthening and nucleus movement during tissue morphogenesis. *Proc. Natl. Acad. Sci. U.S.A.* **109**, 19298-19303.

Giurumescu, C. A., Kang, S., Planchon, T. A., Betzig, E., Bloomekatz, J., Yelon, D., Cosman, P. and Chisholm, A. D. (2012). Quantitative semi-automated analysis of morphogenesis with single-cell resolution in complex embryos. *Development* **139**, 4271-4279.

Keller, P. J. (2013). Imaging morphogenesis: technological advances and biological insights. *Science* **340**, 1234168.

Khairy, K. and Keller, P. J. (2011). Reconstructing embryonic development. *Genesis* **49**, 488-513.

Krzic, U., Gunther, S., Saunders, T. E., Streichan, S. J. and Hufnagel, L. (2012). Multiview light-sheet microscope for rapid in toto imaging. *Nat. Methods* **9**, 730-733.

Lecuit, T. and Lenne, P.-F. (2007). Cell surface mechanics and the control of cell shape, tissue patterns and morphogenesis. *Nat. Rev. Mol. Cell Biol.* **8**, 633-644.

McMahon, A., Supatto, W., Fraser, S. E. and Stathopoulos, A. (2008). Dynamic analyses of Drosophila gastrulation provide insights into collective cell migration. *Science* **322**, 1546-1550.

Morin, X., Daneman, R., Zavortink, M. and Chia, W. (2001). A protein trap strategy to detect GFP-tagged proteins expressed from their endogenous loci in Drosophila. *Proc. Natl. Acad. Sci. U.S.A.* **98**, 15050-15055.

Mosaliganti, K. R., Noche, R. R., Xiong, F., Swinburne, I. A. and Megason, S. G. (2012). ACME: automated Cell Morphology Extractor for comprehensive reconstruction of cell membranes. *PLoS Comput. Biol.* **8**, e1002780.

Müller, H. A. and Wieschaus, E. (1996). armadillo, bazooka, and stardust are critical for early stages in formation of the zonula adherens and maintenance of the polarized blastoderm epithelium in Drosophila. *J. Cell Biol.* **134**, 149-163.

Nelson, K. S., Khan, Z., Molnár, I., Mihály, J., Kaschube, M. and Beitel, G. J. (2012). Drosophila Src regulates anisotropic apical surface growth to control epithelial tube size. *Nat. Cell Biol.* **14**, 518-525.

Development (2014) 141, 2895-2900 doi:10.1242/dev.107730

Oates, A. C., Gorfinkiel, N., González-Gaitán, M. and Heisenberg, C.-P. (2009). Quantitative approaches in developmental biology. *Nat. Rev. Genet.* **10**, 517-530.

Oda, H. and Tsukita, S. (2001). Real-time imaging of cell-cell adherens junctions reveals that Drosophila mesoderm invagination begins with two phases of apical constriction of cells. *J. Cell Sci.* **114**, 493-501.

Olivier, N., Luengo-Oroz, M. A., Duloquin, L., Faure, E., Savy, T., Veilleux, I., Solinas, X., Debarre, D., Bourgine, P., Santos, A. et al. (2010). Cell lineage reconstruction of early zebrafish embryos using label-free nonlinear microscopy. *Science* **329**, 967-971.

Paluch, E. and Heisenberg, C.-P. (2009). Biology and physics of cell shape changes in development. *Curr. Biol.* **19**, R790-R799.

Pandey, R., Heidmann, S. and Lehner, C. F. (2005). Epithelial re-organization and dynamics of progression through mitosis in Drosophila separase complex mutants. *J. Cell Sci.* **118**, 733-742.

Sherrard, K., Robin, F., Lemaire, P. and Munro, E. (2010). Sequential activation of apical and basolateral contractility drives ascidian endoderm invagination. *Curr. Biol.* **20**, 1499-1510.

Szeliski, R. (2011). Computer Vision: Algorithms and Applications. *Berlin*: Springer.

Tomer, R., Khairy, K., Amat, F. and Keller, P. J. (2012). Quantitative high-speed imaging of entire developing embryos with simultaneous multiview light-sheet microscopy. *Nat. Methods* **9**, 755-763.

Truong, T. V., Supatto, W., Koos, D. S., Choi, J. M. and Fraser, S. E. (2011). Deep and fast live imaging with two-photon scanned light-sheet microscopy. *Nat. Methods* **8**, 757-760.

Wang, Y.-C., Khan, Z., Kaschube, M. and Wieschaus, E. F. (2012). Differential positioning of adherens junctions is associated with initiation of epithelial folding. *Nature* **484**, 390-393.

Wang, Y.-C., Khan, Z. and Wieschaus, E. F. (2013). Distinct Rap1 activity states control the extent of epithelial invagination via α-Catenin. *Dev. Cell* **25**, 299-309.